



# Effect of hydrous manganese oxide (HMO) functional groups on oily wastewater treatment

Nor Hafiza Ismail<sup>1,2</sup> · Wan Norharyati Wan Salleh<sup>1,2</sup> · Hasrinah Hasbullah<sup>1,2</sup> · Ahmad Fauzi Ismail<sup>1,2</sup>

Received: 23 August 2022 / Accepted: 11 April 2023 / Published online: 4 May 2023  
© King Abdulaziz City for Science and Technology 2023

## Abstract

The innovative exploitation of diverse inorganic materials in environmental applications has received great scientific attention as a result of the rapid growth of nanotechnology and the expanding variety of nanomaterials currently being produced and developed. The idea of developing multifunctional nanocomposite membranes that can do more than just separate things has been made possible using inorganic nanoparticles as fillers in polymeric matrix. In this work, the nanocomposite was utilized to separate an oil/water emulsion. With the intention of enhancing the capabilities of PVDF-based membrane for oil/water emulsion filtration, synthesized hydrous manganese oxide (HMO) nanoparticles were mixed with poly(vinylidene fluoride) (PVDF) polymer to form mixed matrix membrane (MMM). With the addition of HMO nanoparticles, the MMM showed that the membrane wetting properties, hydrophilicity and oleophobicity, were greatly improved owing to the high amount of –OH functional groups. Subsequently, the improved surface hydrophilicity leads to greater water flux of PVDF/HMO MMM ( $402.0 \pm 11.75 \text{ L/m}^2 \text{ h}$ ; oil rejection efficiency = 93.8%) in comparison to pristine PVDF membrane ( $42.4 \pm 3.73 \text{ L/m}^2 \text{ h}$ ; oil rejection efficiency = 96.2%). Furthermore, compared to pristine PVDF membrane, the flux recovery rate (FRR) and reversible fouling ( $R_r$ ) of the MMM were increased by two–three times, while the irreversible fouling ( $R_{ir}$ ) was reduced by half. This demonstrates that the HMO nanoparticles in the nanocomposite improved the water affinity and reduced low possibility of fouling problem. Hence, the modified nanocomposite membrane can be applied in oily wastewater treatment and competed with the current technologies.

**Keywords** HMO nanoparticles · Mixed matrix membrane · Oily wastewater · Oil/water emulsion · Hydrophilic membrane

## Introduction

Industrial waste containing oil has negative consequences on both the human health and the environment (Kundu and Mishra 2018; Adetunji and Olaniran 2021; Corti-Monzón et al. 2020; Singh et al. 2020). The necessity to identify efficient treatment for oil/water separation, which is a global concern, must be addressed immediately (Sultana and Rahman 2022). Oily wastewater is produced from a variety of sources, and as a result, its chemical composition, and

physical features, such as size, surface charge, and content, may vary. It is important to remove the foulants—in this study, oil droplets from the oily wastewater to obtain cleaner sources of water and to reduce the causes of environmental pollution. Membrane separation is a technology that has received much interest due to its high separation efficiency and low energy usage in many emulsion separation applications (Ismail et al. 2021; Liu et al. 2019; Sliesarenko et al. 2020). However, polymer-based membranes typically have hydrophobic and oleophilic properties that make it unsuitable for use in oily wastewater due to their susceptibility to extreme fouling issues.

Due to their excellent membrane-forming capabilities, resistance to a wide pH range, and chemical stability, polymeric-based membranes, such as poly(vinylidene fluoride) (PVDF), polyacrylonitrile (PAN), and polyethersulfone (PES), are the most often used polymers for symmetric membranes. The biggest drawback to its use in oil/water separation is that it has a high propensity to cause severe

✉ Wan Norharyati Wan Salleh  
hayati@petroleum.utm.my

<sup>1</sup> Advanced Membrane Technology Research Centre (AMTEC), Universiti Teknologi Malaysia, 81310 Skudai, Johor Darul Takzim, Malaysia

<sup>2</sup> Faculty of Chemical and Energy Engineering, Universiti Teknologi Malaysia, 81310 Skudai, Johor Darul Takzim, Malaysia

oil fouling (Asad et al. 2021; Adetunji and Olaniran 2021). One strategy for resolving this matter is to combine hydrophilic materials with polymers, as these properties offer good benefits for separating oil/water emulsions (Ismail et al. 2020b; Awad et al. 2021; Zhan et al. 2021). Hydrophilic nanoparticles can produce a fouling resistant surface that could mitigate the adhesion of oil droplets and facilitate the detachments of the foulants. Generally, hydrophilic materials contain negative functional groups (i.e., hydroxyl (–OH), carboxyl (–COOH)) that help to increase the repellency force (Chen et al. 2021; Shen et al. 2021).

Many works have reported the positive impacts of incorporating hydrophilic nanoparticles on separating oil/water emulsion to obtain clean water. The presence of hydrophilic characteristics reassures the formation of hydration layer during separation performance, which induces higher water affinity and creates a layer that eludes oil droplets from adhering to the membrane surface (Han et al. 2019; Ullah et al. 2021; Ghorbani et al. 2021; Liu et al. 2019). This layer interrupts the interaction of oil droplets and membrane, thereby repelling the deposition of the foulants. One of the inevitable issues in membrane filtration system is membrane fouling (Guo et al. 2018). Thus, most previous works focused on generating hydrophilic and oleophobic membrane, as this could lessen the possibility of oil droplets from blocking the membrane pores, which would eventually create a cake layer on the membrane (Huang et al. 2018; Bengani-Lutz et al. 2017).

Matindi et al. (2021) fabricated the polyethersulfone (PES)/sulfonated polysulfone (SPSf)/titanium oxide (TiO<sub>2</sub>) mixed matrix membrane (MMM) via non-solvent-induced phase separation (NIPS) technique. The aim of their study was to tailor the relationship between pore structure and the requisite properties during separation oil/water emulsion by investigating for a suitable balance for both polymers and additives. The TiO<sub>2</sub> was the most often selected additive in many researches due to its outstanding nanoparticles for improving the membrane hydrophilicity and its antifouling properties (Lai et al. 2017). The MMM fabricated by Matindi et al. (2021) managed to attain pure water flux at 555.3 L/m<sup>2</sup>.h.bar with 90% oil rejection and permeance recovery rate (PRR) at 89.5% at initial concentration of 900 ppm. The incorporation of TiO<sub>2</sub> in the MMM improved the membrane hydrophilicity, as the water droplet completely disappeared (i.e., penetrated into the membrane) within 100 s, compared to its pristine membrane that obtained water contact angle at 36° at the same time. This shows that the addition of nanoparticles in the MMM managed to enhance the water affinity of the membrane and water molecules (Yong et al. 2019; Deng et al. 2019).

The hydrophilic nanoparticles that act as the MMM additives are responsible for both reducing the fouling issue and initiating superior wetting properties (hydrophilic and

oleophobic) (Adetunji and Olaniran 2021). De Guzman et al. (2021) employed polydopamine-sulfobetaine methacrylate P(DA-SBMA) in cellulose acetate (CA) membrane via wet-phase inversion. The P(DA-SBMA) nanoparticles were synthesized from dopamine (DA) and sulfobetaine methacrylate (SBMA) using a controlled ratio of DA and SBMA. The addition of P(DA-SBMA) increased the MMM hydrophilicity from 60° ± 2.78° to 54.29° ± 1.91° and oleophobicity from 121.97° ± 2.16° to 130.41° ± 2.38° owing to the abundance hydrophilic functional groups present in the synthesized nanoparticles (Pandele et al. 2018). Based on the study, the water flux was obtained at 583.64 ± 25.12 L/m<sup>2</sup> h and oil separation efficiency greater than 95%. In addition, the fabricated MMM exhibited a remarkable antifouling property with flux recovery rate (FRR) at 84.17 ± 2.04%, R<sub>r</sub> = 67.59 ± 3.35%; R<sub>ir</sub> = 15.83 ± 2.04%. This proved that the membrane was less susceptible to fouling, as the hydrophilic properties had given it a number of advantages (Ao et al. 2017; Zarghami et al. 2019).

Herein, to prepare the promising MMM for oil/water emulsion, self-synthesized hydrous manganese oxide (HMO) was utilized and incorporated with poly(vinylidene fluoride) (PVDF) polymer. Previously, HMO was used for heavy metal adsorption but due to its exceptional properties, it is deemed suitable for application in oily wastewater treatment, i.e., high amount of hydroxyl (–OH) groups (Delavar et al. 2017). As aforementioned, the abundance amount of hydroxyl groups had induced great attraction between the membrane and water molecules, where it also work as a barrier layer to reduce the chances of oil droplets adhering to the membrane surface and prevent the formation of cake layer (Tummons et al. 2020). Moreover, the surface roughness value was affected by the presence of HMO; the HMO smoothed out the MMM surface, reducing the risk of severe fouling. The PVDF/HMO MMM was prepared via non-solvent induced phase (NIPS) and the MMM was compared with its pristine membrane in this work. The characteristics and flux performance of the membranes was compared and discussed in Sect. “Results and discussion”.

## Experimental

### Materials

The PVDF (Kynar @ 760) pellets (Arkema Inc., Philadelphia, USA) was used as host polymer and N-Methyl-2-Pyrrolidone (NMP) (Merck, > 99%) as dope solvent. Meanwhile, the HMO nanoparticles were synthesized using manganese(II) sulfate monohydrate (MnSO<sub>4</sub>·H<sub>2</sub>O), potassium permanganate (KMnO<sub>4</sub>), and sodium hydroxide (NaOH) from Merck. Glycerol (Merck, > 99.5%) was used for post-treatment.

## Synthesis of HMO nanoparticles

The HMO nanoparticles were synthesized using a method by Parida et al. (1981), which was generated via the oxidation of manganese ions. First, potassium permanganate ( $\text{KMnO}_4$ ) was dissolved in deionized water. After obtaining a homogeneous  $\text{KMnO}_4$  solution, 1 M of sodium hydroxide ( $\text{NaOH}$ ) was added until the pH of the solution reached 12.5. Manganese(II) sulfate monohydrate ( $\text{MnSO}_4 \cdot \text{H}_2\text{O}$ ) was dissolved in deionized water in another beaker. Then, the  $\text{KMnO}_4$  solution was added dropwise in the  $\text{MnSO}_4 \cdot \text{H}_2\text{O}$  solution under vigorous stirring. Once the two solutions came into contact, a brown precipitate (HMO) was formed. The resulting nanoparticles were rinsed until the pH level reached 7, which then aged for three weeks. Subsequently, the HMO nanoparticles were dried in a vacuum oven for 24 h at 65 °C. Lastly, HMO nanoparticles were ground and sieved before they were placed and stored in a desiccator. The Malvern Zetasizer Nano ZSP was used to measure average diameter of HMO that was obtained at 178.9 nm.

## Membrane fabrication

HMO nanoparticles at a concentration of 10 wt% were stirred in the NMP at 60 °C until the HMO was thoroughly diluted in the solvent. The solution was then gradually added with 18 wt% of PVDF until a homogeneous mixture was achieved. After that, the solution was placed in a sonicator to eliminate the bubbles formed during the stirring process. Similar technique was used to prepare the pristine PVDF membrane, where the PVDF dope solution was prepared under the same condition— a mixture of PVDF polymers and NMP.

The homogenous dope solution was poured onto a glass plate, cast with a roller glass to form a flat sheet, and then immersed in tap water. The membrane was transferred to a different coagulation bath after naturally delaminating off from the glass plate. Next, the membranes were immersed in glycerol at a 1:4 ratio of glycerol to water. Finally, the membranes were dried overnight in an oven at 40 °C.

## Characterization

The functional groups on the membrane surface were analyzed using Fourier-transform infrared spectrometry (FTIR). A scanning electron microscope (SEM; model JEOL JSM-5610LV) was used to inspect the cross-section morphology of the membrane. The MMM was subjected to elemental analysis via energy-dispersive X-ray (EDX) spectrometry. The parameters of membrane surface roughness were determined using the tapping mode of an atomic force microscope (AFM; model NX-Hivac), with a scan area of  $10 \mu\text{m} \times 10 \mu\text{m}$ . A Goniometers (OCA 15Pro, Data Physics)

were utilized to measure the water- and oil-contact angles, respectively, of the wetting properties. Meanwhile, RO water and lubricating oil were used as probe liquid. To account for the impact of surface roughness on the wetting properties, the water contact angle was re-calculated using the Wenzel method in Eq. 1.

$$\cos \theta_w = r \cos \theta_Y, \quad (1)$$

where  $\theta_w$  is the Wenzel contact angle, and  $\theta_Y$  is the smooth contact angle and  $r$  is the ratio between the real surface area and the projected surface area of a rough surface (Zhu and Li 2015; Ismail et al. 2021).

## Membrane filtration test

Lubricant oil, sodium dodecyl sulfate (SDS), and deionized water were mixed to create a synthetic oil/water emulsion (1000 ppm), in which SDS was used to stabilize the solution and inhibit the coalescence of the oil droplets. The ratio of lubricant oil to SDS was 9:1 (w/w). The size of the oil droplets was determined to be 80.72 nm (8.90%), 132.18 nm (90.00%), and 412.00 nm (1.10%), all of which were measured using the Malvern Zetasizer Nano ZSP.

The flux value in this work was attained from a cross-flow system. To achieve steady state and prevent a dramatic decline in flux, the membranes were first compressed at 2 bar for 1 h. The flux value ( $J_w$ ,  $\text{L}/\text{m}^2 \text{ h}$ ) was determined using Eq. 2 at 1 bar. Every reading of the flux value was recorded for 10 min.

$$J_w = \frac{Q}{A \times \Delta T}, \quad (2)$$

where  $Q$  is the volume of permeate collected over a specific time ( $L$ ),  $A$  is the membrane effective surface area ( $\text{m}_2$ ), and  $\Delta T$  is the sampling time ( $h$ ).

The oil rejection efficiency was calculated as per Eq. 3.

$$R\% = \left( \frac{C_f - C_p}{C_f} \right) \times 100, \quad (3)$$

where  $R$  is the process of rejection (%),  $C_p$  is the concentration of the permeate (%), and  $C_f$  is the concentration of the feed (%). The oil concentration was determined by UV–Vis spectrophotometer (UV-3101PC model) at a wavelength of 320 nm for oil water concentration of 1000 ppm.

The FRR was evaluated with Eq. (4).

$$\text{FRR}(\%) = \left( \frac{J_{w2}}{J_{w1}} \right) \times 100\%, \quad (4)$$

where  $J_{w1}$  and  $J_{w2}$  ( $\text{L}/\text{m}^2 \text{ h}$ ) are the pure water flux before and after filtration of 1000 ppm oil/water emulsion, respectively. The FRR value indicates the ability of the membrane

to maintain its performance after undergoing oil/water emulsion-pure water–oil/water emulsion cycle.

The flux loss due to reversible ( $R_r$ ) and irreversible ( $R_{ir}$ ) fouling of the membranes is calculated using Eqs. 5–Eq. 7. The oil layer formed on the membrane surface can easily be removed by the backwash or flushing method, which is presented as  $R_r$ . Meanwhile,  $R_{ir}$  is pore-blocking fouling that can be removed by chemical cleaning (Nawi et al. 2021; Nnadiokwe et al. 2021). However, in this research, both  $R_r$  and  $R_{ir}$  flux losses were evaluated by water flushing. The flux loss is calculated using the following equations:

$$R_t(\%) = \left(1 - \frac{J_{oil}}{J_{w1}}\right) \times 100\%, \quad (5)$$

$$R_r(\%) = \left(\frac{J_{w2} - J_{oil}}{J_{w1}}\right) \times 100\%, \quad (6)$$

$$R_{ir}(\%) = \left(\frac{J_{w1} - J_{w2}}{J_{w1}}\right) \times 100\%, \quad (7)$$

where  $R_t$  is the degree of total flux loss caused by total fouling. Meanwhile,  $R_r$  and  $R_{ir}$  represent the irreversible and reversible fouling resistances on the surface and in the pores, respectively.  $J_{oil}$  ( $L/m^2 h$ ) is the flux for oil/water emulsion, while  $J_{w1}$  and  $J_{w2}$  ( $L/m^2 h$ ) are as referred in Eq. 4.

## Results and discussion

### Surface chemical composition

The ATR-FTIR spectra were generated for HMO, pristine PVDF membrane, and PVDF/HMO MMM as displayed in Fig. 1a. This characteristic further corroborated the presence of HMO in the MMM and was used to compare the

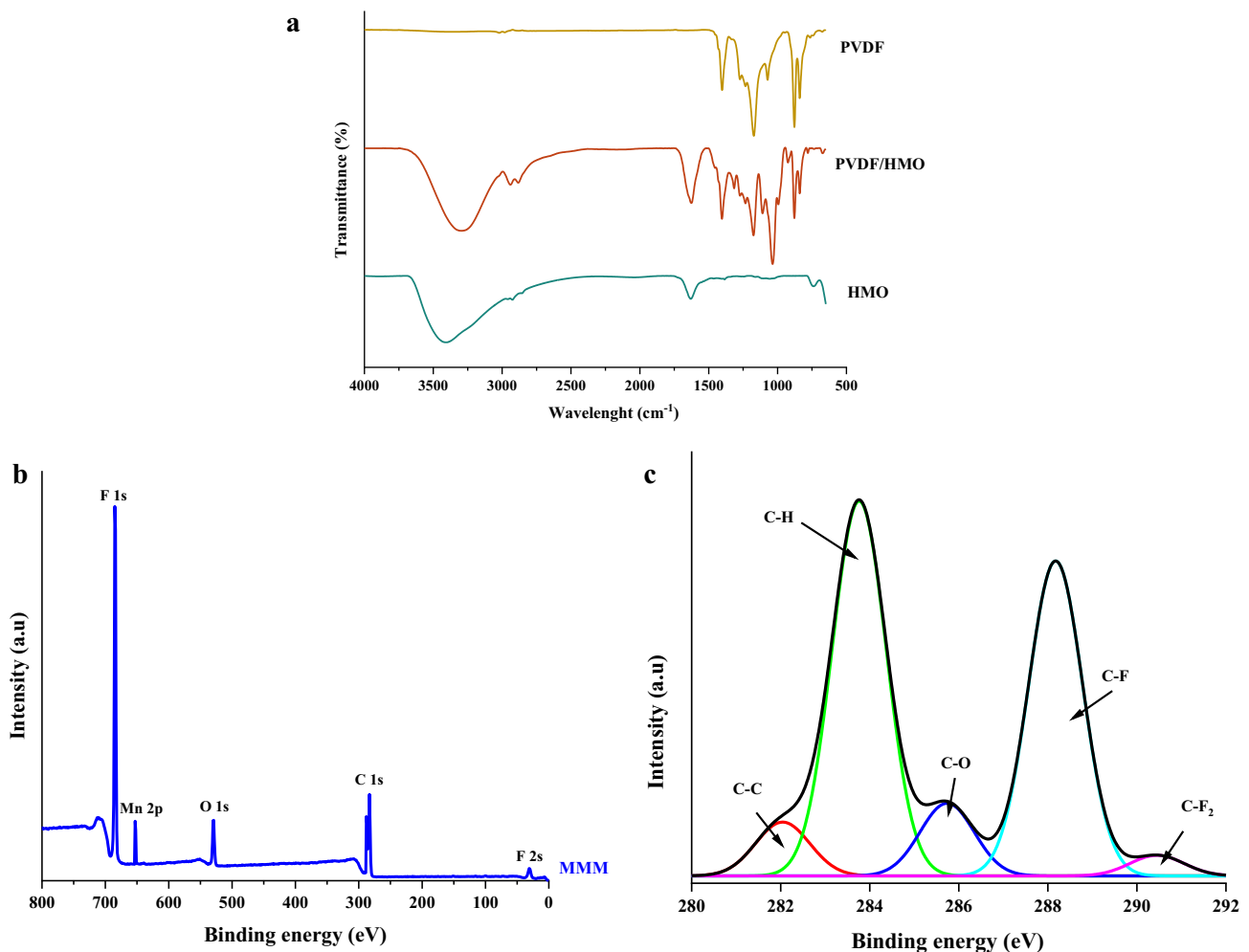


**Fig. 1** a The ATR-FTIR of HMO nanoparticle, PVDF membrane, and PVDF/HMO MMM showing their corresponding functional groups, b XPS wide scan and c C1s spectra of the PVDF/HMO MMM

difference between pristine PVDF and PVDF/HMO membrane. The peak at  $3400\text{ cm}^{-1}$  in HMO was observed, as the HMO is known for its abundant number of  $-\text{OH}$  (hydroxyl) groups (Gohari et al. 2014, Ismail et al. 2020a). This  $\text{O}-\text{H}$  vibration increases the affinity of water on the membrane surface. HMO also showed stretching vibration at  $2940\text{ cm}^{-1}$  and  $2890\text{ cm}^{-1}$  of  $\text{C}-\text{H}$  and  $\sim 720\text{ cm}^{-1}$  represents the  $\text{MnO}_6$  octahedra (Delavar et al. 2017; Wan et al. 2014). In addition, the band at  $1630\text{ cm}^{-1}$  was attributed to  $\text{O}-\text{H}$  and Mn atoms (Vetrivel et al. 2019). Meanwhile, pristine PVDF membrane peaks were observed in the range of  $509\text{--}1406\text{ cm}^{-1}$ . According to Salimi and Yousefi (2003), they specified that the peaks  $509\text{ cm}^{-1}$  and  $840\text{ cm}^{-1}$  were an indication of  $\beta$ -phase formation and  $530, 841, \text{ and } 873\text{ cm}^{-1}$  were evidence of high content of  $\alpha$ -phase. However, peak higher than  $1000\text{ cm}^{-1}$  was not further discussed in the report. Besides that, very weak peaks at  $1700\text{ cm}^{-1}$  and  $3000\text{ cm}^{-1}$  were polymer chain defects caused by the head-to-head and tail-to-tail linkages (Boccaccio et al. 2002). All functional groups that were present in both the PVDF membrane and HMO were present in the PVDF/HMO MMM, demonstrating the deposition of HMO into the MMM. The  $\alpha$  and  $\beta$  phases in PVDF/HMO remain similar peak to that of PVDF membrane, as well as that of the Mn  $\text{C}-\text{H}$  stretching vibration in HMO. Meanwhile, the  $\text{O}-\text{H}$  stretching vibration of the MMM was observed at peak  $3300\text{ cm}^{-1}$ . The PVDF/HMO functional groups confirmed the successful introduction of HMO into the MMM. Further examine of MMM in term of chemical composition was carried out using XPS as shown in Fig. 1b and c. F 1 s, Mn 2 p, O 1 s, C 1 s and F 2 s peaks appeared in MMM for XPS wide spectra. The C 1 s of MMM was deconvoluted into  $\text{C}-\text{C}$  ( $282.09\text{ eV}$ ),  $\text{C}-\text{H}$  ( $283.75\text{ eV}$ ),  $\text{C}-\text{O}$  ( $285.83\text{ eV}$ )  $\text{C}-\text{F}$  ( $288.19\text{ eV}$ ) and  $\text{C}-\text{F}_2$  ( $290.50\text{ eV}$ ) representing the mainly existence of composition on the modified membrane.

### Morphological analysis

Figure 2 displays the membrane surface view and cross section of PVDF and PVDF/HMO MMM, as well as EDX mapping and the elemental spectrum of the MMM. Based on the surface view, the pristine PVDF membrane showed rough surface comparing to the MMM. The agglomeration on the surface of the membranes was due to the residue of the post-treatment. A uniform distribution of O and Mn was observed on the membrane surface, as shown in Fig. 2b. The membranes have a typical asymmetric structure with a finger-like structure and a porous skin sublayer. The presence of HMO nanoparticles reduces the polymeric solution's thermodynamic stability during the phase inversion process of membrane fabrication. This allowed for rapid separation between non-solvent and solvent, which had an impact on both membranes' finger-like sizes (Rabiee et al. 2014).

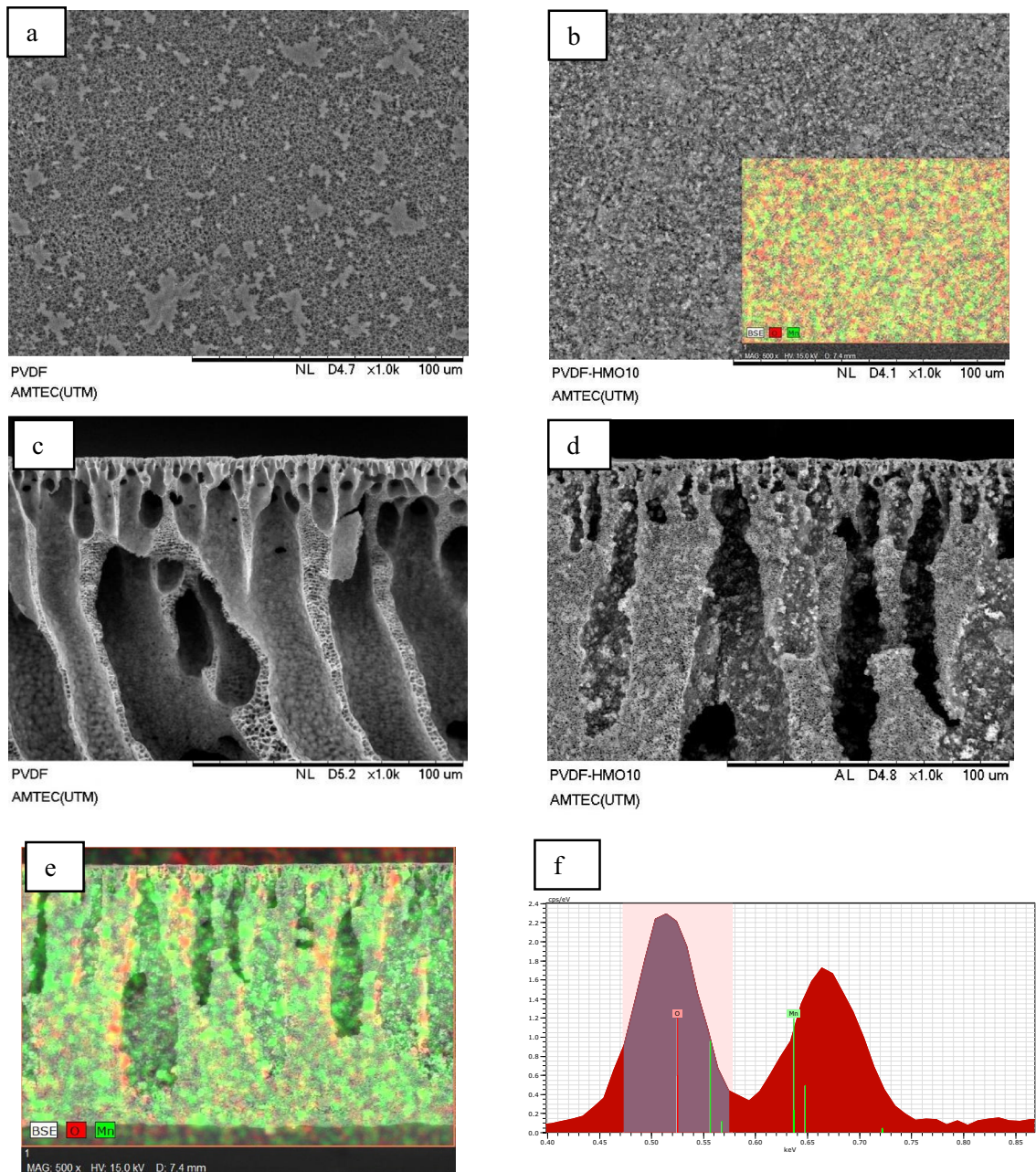
Additionally, the difference between the pristine PVDF and MMM cross-sections allowed for such clear indication the presence of HMO nanoparticles in the MMM. The thickness of the pristine PVDF and PVDF/HMO nanocomposite membrane was obtained at  $282\text{ }\mu\text{m}$  and  $247\text{ }\mu\text{m}$ , respectively, as reported in our previous work (Ismail et al. 2019). The PVDF/HMO MMM showed higher thickness due to the presence of HMO nanoparticle in the dope solution as this affect to higher viscosity. Since HMO nanoparticles were present inside the membrane, their dispersion in the MMM clarified the explanation of the rougher surface there. Figure 2e shows the distribution elements of Mn (green) and O (red) that distributed evenly. The green color dominated the EDX mapping cross section and demonstrated in Fig. 2f elements spectrum, indicating that the Mn:O ratio in the MMM was approximately 3:1. Additionally, the SEM images of HMO were expected to be homogeneous grains reported by Granados Correa and Jiménez-Becerril (2004) as the method used to analyze HMO is similar.

### Surface roughness and wetting behavior

Table 1 presents the surface roughness and wetting characteristics of the membranes. The surface roughness value of the nanocomposite had decreased with the incorporation of HMO nanoparticles. The surface roughness parameters of the membranes were determined by average surface roughness ( $R_a$ ), root-mean-roughness ( $R_q$ ), and average of the tallest peak to the depth of the lowest valley ( $R_z$ ). Smoother membrane surface is preferable as high surface roughness value facilitates the accumulation of oil droplets and, thus, makes vulnerable the membrane to fouling (Zhang et al. 2022). The  $R_a$  of the PVDF and PVDF/HMO was obtained at  $192 \pm 24.94\text{ nm}$  and  $129 \pm 20.92\text{ nm}$ , respectively, which indicated that the HMO existence in the composite membrane has fouling resistance behavior (Huang et al. 2018). The composite membrane surface was smoother than the pristine membrane, although Fig. 2 shows that the HMO nanoparticles generated a coarser cross-section morphology. In addition, the PVDF membrane obtained  $R_q$  and  $R_z$  at  $200.13 \pm 29.67$  and  $1250.14 \pm 159.22$ , respectively. Meanwhile, PVDF/HMO demonstrated  $R_q$  and  $R_z$  at  $180.11 \pm 27.79$  and  $1141.97 \pm 266.67$ , respectively. The PVDF showed higher  $R_z$  due to the high difference between the highest and lowest peaks of the PVDF membrane that is clearly demonstrated in Table 1.

Wenzel explored the correlation between wettability and surface roughness, stating that an increase in surface roughness would magnify the wettability given on by the surface chemistry (Asad et al. 2021). Thus, the water contact angle value was re-calculated using Wenzel method as in Eq. 1. The addition of HMO nanoparticles in the MMM decreased the water contact angle value from  $97^\circ$  to  $67^\circ$ .



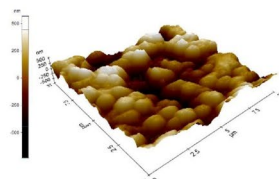
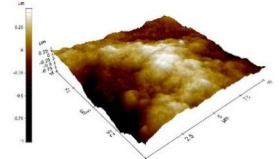


**Fig. 2** Membrane surface view (Ismail et al. 2019, 2020a) and cross-section morphology of **a, c** PVDF membrane, **b, d** PVDF/HMO MMM, **e** EDX mapping of O and Mn, and **f** elements spectrum of MMM

The hydrophobicity of the PVDF membrane was reduced by the existence of –OH functional groups in the HMO nanoparticles. The existence of these functional groups is important for enhancing the attraction of water molecules to pass through the membranes, as the aim of the research was to acquire clean water (Ismail et al. 2020b). On top of that, an anti-oil membrane surface was necessary to increase the membrane’s ability to repel oil droplets while reducing the risk for oil droplets from aggregating on the membrane (Sultana and Rahman 2022; Liu et al. 2019).

The oil-contact-angle value of the PVDF and PVDF/HMO membranes was attained at  $0^\circ$  and  $35.1^\circ$ , respectively. In the determination of the oil-contact-angle value, the oil droplets rapidly penetrated into the PVDF membrane. This was encouraged by the behavior of PVDF because of its inherent preference for oil (Tanis-Kanbur et al. 2018). In this work, the modified MMM was claimed underwater oleophobic, thus Fig. 3 is prepared to prove the ability of membrane has high resisted to oil droplets. First, half of the membrane was placed in air and half was immersed in water. The lubricant

**Table 1** Surface roughness and wetting properties of pristine PVDF and PVDF/HMO membrane

| Membrane | Surface roughness (nm)   | Wetting properties      |                       |
|----------|--|-------------------------|-----------------------|
|          |  | Water contact angle (°) | Oil contact angle (°) |
| PVDF     | <br>$R_a = 192 \pm 24.94$<br>$R_q = 200.13 \pm 29.67$<br>$R_z = 1250.14 \pm 159.22$ | 97.0                    | 0.0                   |
| PVDF/HMO | <br>$R_a = 129 \pm 20.92$<br>$R_q = 180.11 \pm 27.79$<br>$R_z = 1141.97 \pm 266.67$ | 67.0                    | 35.1                  |

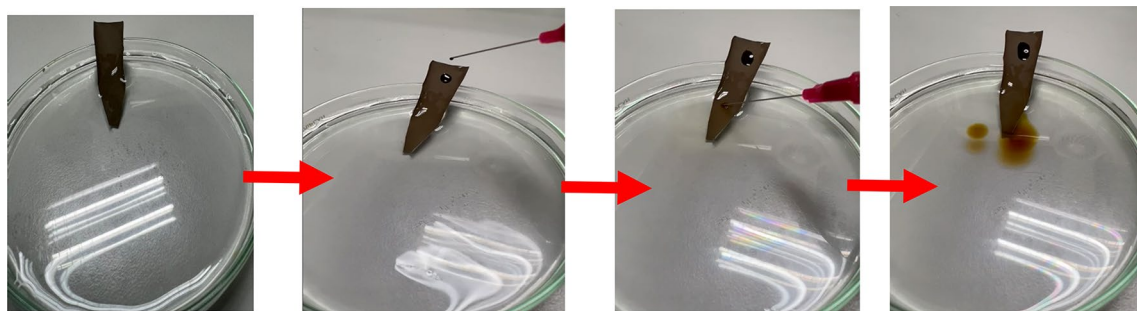


**Fig. 3** Comparing the wetting properties of MMM in air and immersed in water

oil was first dropped on the membrane that exposed in air and after that lubricant oil was dropped on the membrane immersed in water. It can be seen that the oil droplet does not have the possibility to even go near the membrane surface because the modified membrane created hydration layer that repel the attraction of the foulants on the membrane (Zhang et al. 2022).

**Surface charge analysis**

A critical consideration in preventing oil droplets from accumulating on membrane surfaces is the surface charge of the membranes. Surface charge holds the ability to control electrical double-layer (EDL) interaction and so as interfacial tension (Wang et al. 2016). Figure 4 depicts the surface charge of the pristine PVDF and PVDF/HMO MMM. The pristine PVDF membrane displayed approximately positive charge between pH 3.25 and 4 and exhibited a negative charge above pH 4. The PVDF membrane possesses a negative charge by nature when immersed in water with a natural pH (~pH 6–7). Meanwhile, the composite membrane displayed positive charge at pH levels below

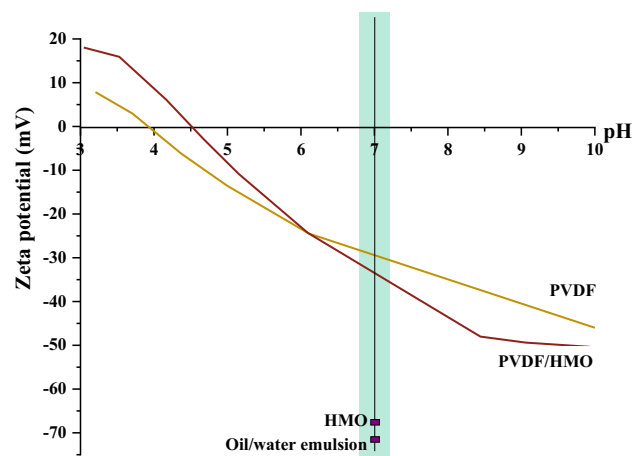


**Fig. 4** Surface charge of PVDF and PVDF/HMO membranes in difference range of pH levels

4.5 and stronger negative charge than PVDF membrane at pH levels above 6. This shows that the addition of HMO nanoparticles in PVDF/HMO MMM demonstrated higher negative value at neutral and based solution (~pH 6–10).

Additionally, when dispersed in water, HMO nanoparticles and 1000 ppm of oil droplets showed zeta potential results at 67.3 mV and  $-72.0$  mV, respectively, which were measured using the Malvern Zetasizer Nano ZSP. The oil droplets are less attracted to the membrane surface due to the negative charges on feed and membranes. Hence, the adherence of oil droplets to the membrane surface can be overcome (Tummons et al. 2017).

### Separation performance of oil/water emulsion

A crossflow filtration system was used to determine the pure water flux, rejection efficiency and oil/water emulsion fluxes of the membranes. The pure water flux and oil rejection efficiency of 1000 ppm oil/water emulsion concentration is shown in Fig. 5a. The pristine PVDF membrane and PVDF/HMO MMM attained water flux at  $42.4 \pm 3.73$  L/m<sup>2</sup> h and

$402.0 \pm 11.75$  L/m<sup>2</sup> h and oil rejection efficiency at 96.2% and 93.8%, respectively. The low flux value of the PVDF membrane was due to the hydrophobicity characteristics that resist the water molecules from passing through. Meanwhile, higher oil rejection efficiency as the oil droplets clogged the PVDF open channels besides its oleophilicity behavior (Abuhasel et al. 2021). The presence of HMO nanoparticles in the composite membrane attracted the water molecules and smoother the passage to pass through the composite membrane, resulted to high water permeability.

Figure 5b shows two cycles of pure water–oil/water emulsion–pure water of the membranes, which each of the separation of pure water and oil/water emulsion was operated for 1 h each. The fluxes of pure water and oil/water emulsion initially showed high water flux value, which then decreased over time for all the tested membranes. Pristine PVDF membrane showed lowest pure water and oil/water emulsion flux.

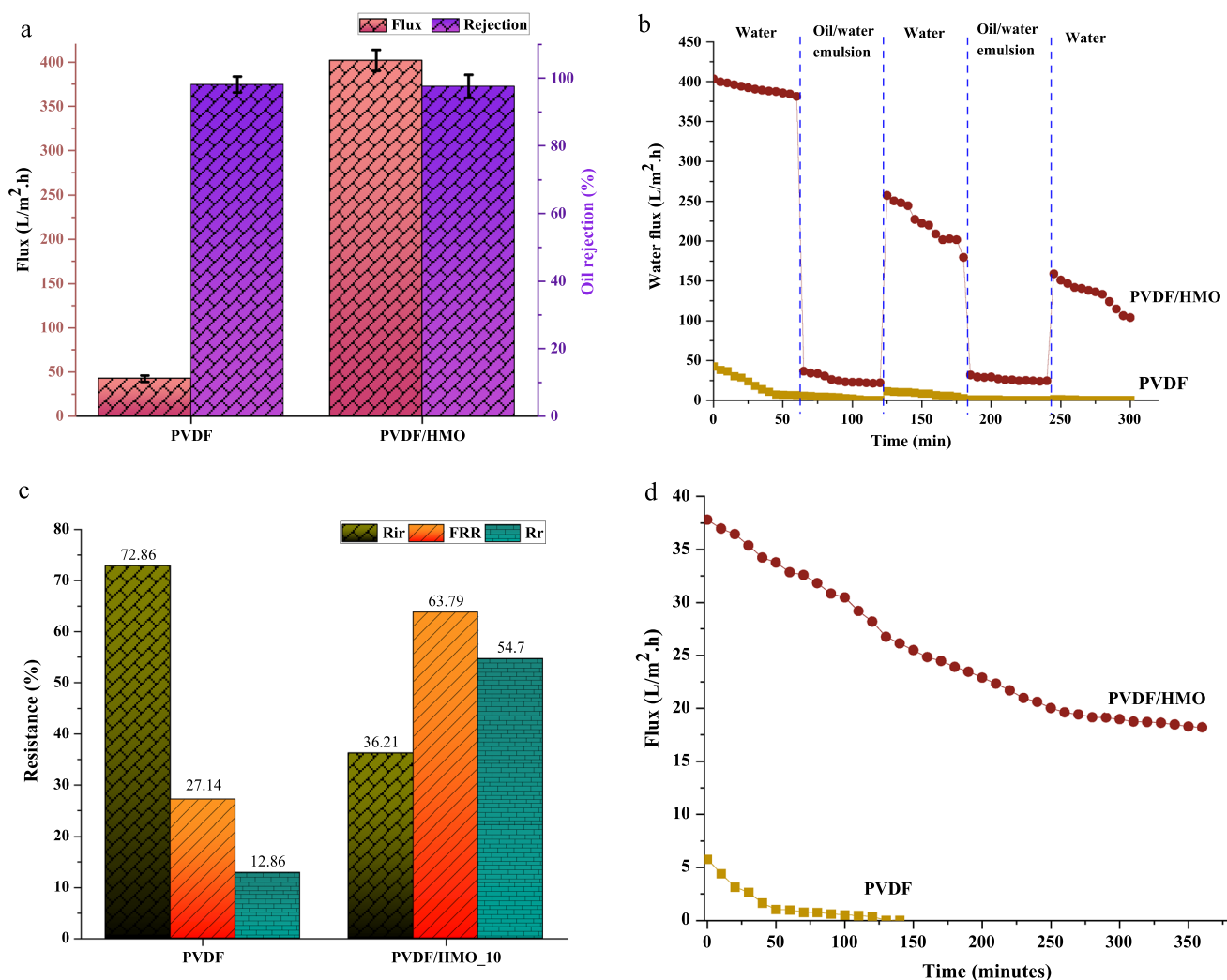


**Fig. 5** a Pure water flux and rejection efficiency, b cycles of pure water–oil/water emulsion–pure water flux, c FRR,  $R_{ir}$  and  $R_r$  percentage and, d time-dependent flux of pristine PVDF and PVDF/HMO membranes



After two times of filtration cycle within 300 min of the total operation, the PVDF membrane and PVDF/HMO MMM declined approximately 99% and 57%, respectively. A flux decline was observed for PVDF especially in separating the oil/water emulsion where the first reading flux was obtained at  $6.11 \text{ L/m}^2 \text{ h}$  that was 6 times lower than the MMM that attained flux at  $36.67 \text{ L/m}^2 \text{ h}$ . The hydrophobic nature of PVDF membrane demote the ability of the water molecules to pass through the membrane (Zhou et al. 2019). Apart from that, the PVDF membrane is oleophilic that allowed the oil droplet to adhere or penetrate into the membrane (Otitoju et al. 2016). Furthermore, once the cake layer had formed, it was difficult to remove the accumulations of oil on the membrane surface, which was reflected in the high  $R_{ir}$  and low FRR value (Fig. 5c) (Ullah et al. 2021). Therefore, the pure water flux in second cycle of PVDF membrane was low, as it was impossible to remove the foulants solely by back-washing and rinsing using water.

The membranes were further analyzed for flux recovery and reversible fouling, as depicted in Fig. 5c, to examine the antifouling properties of the membranes. The FRR,  $R_r$ , and  $R_{ir}$  of the PVDF membrane was gained at 27.14%, 12.86%, and 72.86%, respectively; whereas that of PVDF/HMO membrane was attained at 63.79%, 54.7%, and 36.21%, respectively. As the FRR increases, the  $R_r$  increases correspondingly. The  $R_r$  determines the possibility of the membrane for reuse although it may not perform as well as it does in its original state. Weak repellency of the PVDF membrane is caused by high  $R_{ir}$  value, which indicated poor detachment of the cake layer after back-washing. This phenomenon is caused by the trapped oil on the PVDF membrane, as rough surface leads to severe fouling (Tanis-Kanbur et al. 2018; Ismail et al. 2021; Wang et al. 2020). Due to the oil foulants that were inadequately removed during the washing process, the high  $R_{ir}$  value indicated poor FRR value. On the other hand, the oleophobicity of the MMM made it easier to remove foulant from the membrane surface, as the oil contact angle had increased from  $0^\circ$  to  $35.1^\circ$  (Table 1), which resulted in oil repellency of surfaces (De Guzman et al. 2021). Additionally, the hydration layer produced by the  $-\text{OH}$  functional groups in PVDF/HMO had reduced the possibility of adhesion behavior of oil droplets.

The lifetime of the membranes was conducted for 360 min with using lubricant oil as feed at a concentration of 1000 ppm, as displayed in Fig. 5d. Both membranes showed that the flux declined over time, where pristine PVDF membrane obtained a flux of approximately zero before achieving 150 min of operating time. The inherent hydrophobic nature of PVDF membrane made it susceptible to fouling due to adsorptive surfactants or mechanical pore-plugging by the oil emulsions during the membrane separation process (Li et al. 2018). The oil droplets conquered the membrane surface and formed a layer cake, which led to total fouling with

oil coalescence on the membranes. The MMM with  $-\text{OH}$  functional groups, in contrast, not only enhanced the wetting characteristics but also enhanced the ability to resist oil droplets (Sultana and Rahman 2022). The MMM exhibited more negative charge than pristine PVDF, and had a strong tendency to decrease the possibility of oil droplets adhering to the membrane surface (Mazumder et al. 2020). The nanocomposite membrane, however, also demonstrated flux reduction over time and achieved uniform flux after 300 min because an oil cake layer was formed, impeding the passage of water molecules. Foulant thickness causes an increase in resistance and a decrease in flux. After 360 min of permeating the oil–water emulsion, the PVDF membrane completely collapsed in less than 150 min, and the PVDF/HMO MMM was reduced by 50%.

Figure 6 shows the pristine PVDF and PVDF/HMO membrane after separating oil/water emulsion for 1 h. The wide pores and high level of surface roughness of the PVDF membrane make it highly susceptible to fouling (Matindi et al. 2021). The PVDF membrane with white color evidently showed a cake layer formation on the membrane surface, where the yellow color represents the oil droplets. It can also be seen that the yellow color on the PVDF membrane surface has various yellow tone color, whereby the vivid yellow color of the cake layer represents a thicker cake layer formation on top of the layer and that nearly covered the membrane surface area completely. This occurrence had caused a continuous deposition of oil droplets on the PVDF membrane, drastically reducing its water permeability, lifespan, and risk to severe fouling. Meanwhile, the MMM showed thin layer foulants with small area covered on the membrane surface. This demonstrated the contribution of the HMO nanoparticles employed in the PVDF/HMO. The bonding between the abundant hydroxyl groups from HMO and water molecules was generated by the hydrated layer, where this layer greatly reduced oil droplet attachment on the MMM (Zarghami et al. 2019).

The comparison of current work with previously reported MMMs was presented in Table 2. The operating pressure used was  $\leq 2$  bar using the dead-end or crossflow filtration. Generally, feed without the surfactant (e.g., Tween 80 and

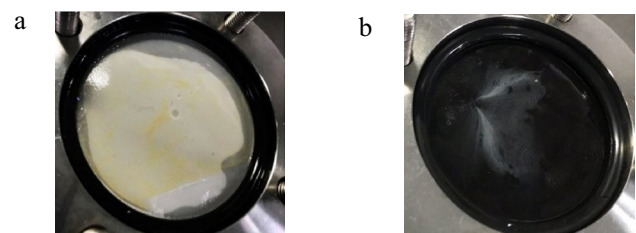


**Fig. 6** **a** PVDF membrane and **b** PVDF/HMO MMM after permeated oil/water emulsion for 1 h

**Table 2** Comparative works in oil/water emulsion separation for MMM

| Materials                      | Operation mode                 | Feed type  | Oil concentration (ppm) | Performance               |                   | References              |
|--------------------------------|--------------------------------|--|-------------------------|---------------------------|-------------------|-------------------------|
|                                |                                |  |                         | Flux (L/m <sup>2</sup> h) | Oil rejection (%) |                         |
| PES/SPSf/TiO <sub>2</sub>      | Crossflow filtration<br>1 bar  | Gasoline: SDS  | 900                     | 555.2                     | 95                | Matindi et al. (2021)   |
| P(DA-SBMA)/CA                  | Crossflow filtration<br>1 bar  | Diesel oil, dodecane, food-grade oil, toluene, hexane: SDS | 1000                    | 583.6                     | 95–99             | De Guzman et al. (2021) |
| PES/SiO <sub>2</sub> -f-MWCNTs | Dead-end filtration<br>0.7 bar | Vegetable oil: Tween 80                                    | 1000                    | 293.9                     | 97                | Hegab et al. (2022)     |
| PES/FePc                       | Crossflow filtration<br>1 bar  | Soy-bean oil: SDS  | 1000                    | 158.9                     | 96.7              | Chen et al. (2018)      |
| PVC/nanoclay                   | Dead-end filtration<br>2 bar   | Crude oil  | 200                     | 186.0                     | 97                | Ahmad et al. (2018)     |
| SiO <sub>2</sub> -g-EGMA/PVDF  | Dead-end filtration<br>2 bar   | Crude oil  | 100                     | 29.4                      | 89                | Saini et al. (2019)     |
| PVDF/HMO                       | Crossflow filtration<br>1 bar  | Lubricant oil: SDS   | 1000                    | 402.0                     | 93.8              | Current work            |

SDS) has higher potential to accumulate and the membrane able to achieve excellent result compared to the feed with surfactant due to the stable oil/water emulsion (Zhou et al. 2019). Additionally, different type of oil has different viscosity which also affects the flux performance. Based on Table 2, it can be seen that the PVDF/HMO membrane demonstrated comparable result in both flux and oil rejection performance in the literature.

## Conclusion

The nanocomposite membrane was prepared via non-solvent-induced phase separation (NIPS) incorporated with HMO nanoparticles. The addition of HMO nanoparticles in the PVDF/HMO MMM improved the membrane hydrophilicity, oleophobicity, and reduced surface roughness, which induced high flux and improved the antifouling properties of the membrane. The abundance of –OH functional groups in the HMO nanoparticles employed in this work prepared the PVDF/HMO MMM required for the treatment of oily wastewater. The presence of HMO nanoparticles in the nanocomposite was confirmed by FTIR and EDX, where a uniform distribution of O and Mn element can be seen in Fig. 1, and the –OH functional groups were determined via FTIR at a wavelength of 3400 cm<sup>-1</sup>. Meanwhile, the PVDF/HMO MMM exhibited water flux at 402.0 ± 11.75 L/m<sup>2</sup> h with an oil rejection efficiency at 93.8% that is 10 times higher than the pristine membrane. The membranes were then subjected to antifouling testing. The PVDF membrane displayed FRR, R<sub>r</sub>, and R<sub>ir</sub> at 27.14%, 12.86%, and 72.86%, respectively. Meanwhile, the PVDF/HMO MMM displayed FRR, R<sub>r</sub>, and R<sub>ir</sub> at 63.79%, 54.70%, and 36.21%, respectively. The PVDF

membrane's poor antifouling properties, which were affected by its high surface roughness value and wetting characteristics—hydrophobic and oleophilic—had led to the formation of cake layer during filtration, as shown by the low FRR and R<sub>r</sub> values of the pristine membrane. On the other hand, the PVDF/HMO showed high flux recovery and reversible fouling values, indicating that the fabricated nanocomposite membrane has good antifouling properties, which can lead to good flux performance.

**Acknowledgements** The authors would like to thank the Ministry of Education and Universiti Teknologi Malaysia for the financial support provided under Fundamental Research Grant Scheme Fundamental Research Grant Scheme (FRGS/1/2020/STG05/UTM/02/1, VOT NO. 5F369) and UTM High Impact Research Grant (Project Number: Q.J130000.2451.08G36) in completing this work. Nor Hafiza Ismail would like to acknowledge the support from Universiti Teknologi Malaysia for the ZAMALAH scholarship.

**Data availability** The data reported in this article are available.

## Declarations

**Conflict of interest** On behalf of all authors, the corresponding author states that there is no conflict of interest.

## References

- Abuhasel K, Kchaou M, Alquraish M, Munusamy Y, Jeng YT (2021) Oily wastewater treatment: overview of conventional and modern methods, challenges, and future opportunities. *Water* 13:980
- Adetunji AI, Olaniran AO (2021) Treatment of industrial oily wastewater by advanced technologies: a review. *Appl Water Sci* 11:98. <https://doi.org/10.1007/s13201-021-01430-4>
- Ahmad T, Guria C, Mandal A (2018) Synthesis, characterization and performance studies of mixed-matrix poly (vinyl

- chloride)-bentonite ultrafiltration membrane for the treatment of saline oily wastewater. *Process Saf Environ Prot* 116:703–717
- Ao C et al (2017) Superhydrophilic graphene oxide@electrospun cellulose nanofiber hybrid membrane for high-efficiency oil/water separation. *Carbohydr Polym* 175:216–222. <https://doi.org/10.1016/j.carbpol.2017.07.085>
- Asad A, Rastgar M, Sameoto D, Sadrzadeh M (2021) Gravity assisted super high flux microfiltration polyamide-imide membranes for oil/water emulsion separation. *J Membr Sci* 621:119019. <https://doi.org/10.1016/j.memsci.2020.119019>
- Awad ES, Sabirova TM, Tretyakova NA, Alsalhy QF, Figoli A, Salih IK (2021) A mini-review of enhancing ultrafiltration membranes (UF) for wastewater treatment: performance and stability. *ChemEngineering* 5:34
- Bengani-Lutz P, Zaf RD, Culfaz-Emecen PZ, Asatekin A (2017) Extremely fouling resistant zwitterionic copolymer membranes with ~ 1nm pore size for treating municipal, oily and textile wastewater streams. *J Membr Sci* 543:184–194. <https://doi.org/10.1016/j.memsci.2017.08.058>
- Boccaccio T, Bottino A, Capannelli G, Piaggio P (2002) Characterization of PVDF membranes by vibrational spectroscopy. *J Membr Sci* 210:315–329. [https://doi.org/10.1016/S0376-7388\(02\)00407-6](https://doi.org/10.1016/S0376-7388(02)00407-6)
- Chen F, Shi X, Chen X, Chen W (2018) An iron (II) phthalocyanine/poly(vinylidene fluoride) composite membrane with antifouling property and catalytic self-cleaning function for high-efficiency oil/water separation. *J Membr Sci* 552:295–304. <https://doi.org/10.1016/j.memsci.2018.02.030>
- Chen S et al (2021) Dual-functional superwetable nano-structured membrane: from ultra-effective separation of oil-water emulsion to seawater desalination. *Chem Eng J* 411:128042
- Corti-Monzón G, Nisenbaum M, Villegas-Plazas M, Junca H, Murialdo S (2020) Enrichment and characterization of a bilge microbial consortium with oil in water-emulsions breaking ability for oily wastewater treatment. *Biodegradation* 31:57–72. <https://doi.org/10.1007/s10532-020-09894-y>
- De Guzman MR et al (2021) Increased performance and antifouling of mixed-matrix membranes of cellulose acetate with hydrophilic nanoparticles of polydopamine-sulfobetaine methacrylate for oil-water separation. *J Membr Sci* 620:118881. <https://doi.org/10.1016/j.memsci.2020.118881>
- Delavar M, Bakeri G, Hosseini M (2017) Fabrication of polycarbonate mixed matrix membranes containing hydrous manganese oxide and alumina nanoparticles for heavy metal decontamination: characterization and comparative study. *Chem Eng Res Des* 120:240–253
- Deng Y, Zhang G, Bai R, Shen S, Zhou X, Wyman I (2019) Fabrication of superhydrophilic and underwater superoleophobic membranes via an in situ crosslinking blend strategy for highly efficient oil/water emulsion separation. *J Membr Sci* 569:60–70. <https://doi.org/10.1016/j.memsci.2018.09.069>
- Ghorbani M, Vakili MH, Ameri E (2021) Fabrication and evaluation of a biopolymer-based nanocomposite membrane for oily wastewater treatment. *Mater Today Commun* 28:102560
- Gohari RJ, Halakoo E, Nazri N, Lau W, Matsuura T, Ismail A (2014) Improving performance and antifouling capability of PES UF membranes via blending with highly hydrophilic hydrous manganese dioxide nanoparticles. *Desalination* 335:87–95
- Granados Correa F, Jiménez-Becerril J (2004) Adsorption of 60Co<sup>2+</sup> on hydrous manganese oxide powder from aqueous solution. *Radiochim Acta* 92:105–110. <https://doi.org/10.1524/ract.92.2.105.27459>
- Guo Z-Y, Yuan X-S, Geng H-Z, Wang L-D, Jing L-C, Gu Z-Z (2018) High conductive PPy-CNT surface-modified PES membrane with anti-fouling property. *Appl Nanosci* 8:1597–1606. <https://doi.org/10.1007/s13204-018-0826-5>
- Han L, Tan YZ, Xu C, Xiao T, Trinh TA, Chew JW (2019) Zwitterionic grafting of sulfobetaine methacrylate (SBMA) on hydrophobic PVDF membranes for enhanced anti-fouling and anti-wetting in the membrane distillation of oil emulsions. *J Membr Sci* 588:117196. <https://doi.org/10.1016/j.memsci.2019.117196>
- Hegab HM et al (2022) Designing of amino silica covalently functionalized carboxylic multi-wall carbon nanotubes-based polyethersulfone membranes for enhancing oily wastewater treatment. *J Environ Chem Eng* 10:108667. <https://doi.org/10.1016/j.jece.2022.108667>
- Huang S, Ras RHA, Tian X (2018) Antifouling membranes for oily wastewater treatment: Interplay between wetting and membrane fouling. *Curr Opin Colloid Interface Sci* 36:90–109. <https://doi.org/10.1016/j.cocis.2018.02.002>
- Ismail N et al (2019) PVDF/HMO ultrafiltration membrane for efficient oil/water separation. *Chem Eng Commun* 208:463–473
- Ismail N et al (2020a) Fabrication of PVDF/HMO mixed matrix membrane: effect of HMO loading on oil/water separation. In: IOP conference series: materials science and engineering. IOP Publishing, 052004
- Ismail NH et al (2020b) Hydrophilic polymer-based membrane for oily wastewater treatment: a review. *Sep Purif Technol* 233:116007. <https://doi.org/10.1016/j.seppur.2019.116007>
- Ismail NH, Salleh WNW, Ahmad SZN, Ismail AF (2021) Effect of various operating parameters towards PVDF/HMO mixed matrix membrane performance. *J Environ Chem Eng* 9:105667. <https://doi.org/10.1016/j.jece.2021.105667>
- Kundu P, Mishra IM (2018) Treatment and reclamation of hydrocarbon-bearing oily wastewater as a hazardous pollutant by different processes and technologies: a state-of-the-art review. *Rev Chem Eng* 35:73–108
- Lai G et al (2017) Novel mixed matrix membranes incorporated with dual-nanofillers for enhanced oil-water separation. *Sep Purif Technol* 178:113–121
- Li J-H, Ni X-X, Zhang D-B, Zheng H, Wang J-B, Zhang Q-Q (2018) Engineering a self-driven PVDF/PDA hybrid membranes based on membrane micro-reactor effect to achieve super-hydrophilicity, excellent antifouling properties and hemocompatibility. *Appl Surf Sci* 444:672–690
- Liu Z, Cao R, Wei A, Zhao J, He J (2019) Superflexible/superhydrophilic PVDF-HFP/CuO-nanosheet nanofibrous membrane for efficient microfiltration. *Appl Nanosci* 9:1991–2000. <https://doi.org/10.1007/s13204-019-01014-4>
- Matindi CN et al (2021) Tailoring the morphology of polyethersulfone/sulfonated polysulfone ultrafiltration membranes for highly efficient separation of oil-in-water emulsions using TiO<sub>2</sub> nanoparticles. *J Membr Sci* 620:118868. <https://doi.org/10.1016/j.memsci.2020.118868>
- Mazumder A, Chowdhury Z, Sen D, Bhattacharjee C (2020) Electric field assisted membrane separation for oily wastewater with a novel and cost-effective electrocoagulation and electroflotation enhanced membrane module (ECEFM). *Chem Eng Process Process Intensif* 151:107918. <https://doi.org/10.1016/j.cep.2020.107918>
- Nawi NIM et al (2021) polyvinylidene fluoride membrane via vapour induced phase separation for oil/water emulsion filtration. *Polymers* 13:427
- Nnadike CC et al (2021) Enhanced filtration characteristics and reduced bacterial attachment for reverse osmosis membranes modified by a facile method. *ACS ES&T Water* 1:1136–1144. <https://doi.org/10.1021/acsestwater.0c00168>
- Otitoju T, Ahmad A, Ooi B (2016) Polyvinylidene fluoride (PVDF) membrane for oil rejection from oily wastewater: a performance review. *J Water Process Eng* 14:41–59

- Pandele A et al (2018) Cellulose acetate membranes functionalized with resveratrol by covalent immobilization for improved osseointegration. *Appl Surf Sci* 438:2–13
- Parida KM, Kanungo SB, Sant BR (1981) Studies on MnO<sub>2</sub>—I. Chemical composition, microstructure and other characteristics of some synthetic MnO<sub>2</sub> of various crystalline modifications. *Electrochim Acta* 26:435–443. [https://doi.org/10.1016/0013-4686\(81\)85033-5](https://doi.org/10.1016/0013-4686(81)85033-5)
- Rabiee H, Farahani MHDA, Vatanpour V (2014) Preparation and characterization of emulsion poly (vinyl chloride)(EPVC)/TiO<sub>2</sub> nanocomposite ultrafiltration membrane. *J Membr Sci* 472:185–193
- Saini B, Sinha MK, Dash SK (2019) Mitigation of HA, BSA and oil/water emulsion fouling of PVDF Ultrafiltration Membranes by SiO<sub>2</sub>-g-PEGMA nanoparticles. *J Water Process Eng* 30:100603. <https://doi.org/10.1016/j.jwpe.2018.03.018>
- Salimi A, Yousefi AA (2003) Analysis Method: FTIR studies of  $\beta$ -phase crystal formation in stretched PVDF films. *Polym Testing* 22:699–704. [https://doi.org/10.1016/S0142-9418\(03\)00003-5](https://doi.org/10.1016/S0142-9418(03)00003-5)
- Shen X et al (2021) Surface PEGylation of polyacrylonitrile membrane via thiol-ene click chemistry for efficient separation of oil-in-water emulsions. *Sep Purif Technol* 255:117418
- Singh H, Jain A, Kaur J, Arya SK, Khatri M (2020) Adsorptive removal of oil from water using SPIONs–chitosan nanocomposite: kinetics and process optimization. *Appl Nanosci* 10:1281–1295. <https://doi.org/10.1007/s13204-019-01195-y>
- Sliesarenko V, Tomina V, Dudarko O, Bauman M, Lobnik A, Melnyk I (2020) Functionalization of polymeric membranes with phosphonic and thiol groups for water purification from heavy metal ions. *Appl Nanosci* 10:337–346. <https://doi.org/10.1007/s13204-019-01170-7>
- Sultana N, Rahman R (2022) Electrospun nanofiber composite membranes based on cellulose acetate/nano-zeolite for the removal of oil from oily wastewater. *Emergent Mater* 5:145–153. <https://doi.org/10.1007/s42247-021-00326-y>
- Tanis-Kanbur MB, Velioğlu S, Tanudjaja HJ, Hu X, Chew JW (2018) Understanding membrane fouling by oil-in-water emulsion via experiments and molecular dynamics simulations. *J Membr Sci* 566:140–150. <https://doi.org/10.1016/j.memsci.2018.08.067>
- Tummons EN, Chew JW, Fane AG, Tarabara VV (2017) Ultrafiltration of saline oil-in-water emulsions stabilized by an anionic surfactant: effect of surfactant concentration and divalent counterions. *J Membr Sci* 537:384–395. <https://doi.org/10.1016/j.memsci.2017.05.012>
- Tummons E, Han Q, Tanudjaja HJ, Hejase CA, Chew JW, Tarabara VV (2020) Membrane fouling by emulsified oil: a review. *Sep Purif Technol* 248:116919. <https://doi.org/10.1016/j.seppur.2020.116919>
- Ullah A, Tanudjaja HJ, Ouda M, Hasan SW, Chew JW (2021) Membrane fouling mitigation techniques for oily wastewater: a short review. *J Water Process Eng* 43:102293. <https://doi.org/10.1016/j.jwpe.2021.102293>
- Vetrivel S, Rana D, Sri Abirami Saraswathi MS, Divya K, Kaleekkal NJ, Nagendran A (2019) Cellulose acetate nanocomposite ultrafiltration membranes tailored with hydrous manganese dioxide nanoparticles for water treatment applications. *Polym Adv Technol* 30:1943–1950
- Wan S et al (2014) Selective capture of thallium(I) ion from aqueous solutions by amorphous hydrous manganese dioxide. *Chem Eng J* 239:200–206. <https://doi.org/10.1016/j.cej.2013.11.010>
- Wang Z, Jin J, Hou D, Lin S (2016) Tailoring surface charge and wetting property for robust oil-fouling mitigation in membrane distillation. *J Membr Sci* 516:113–122
- Wang J, Wu Y, Cao Y, Li G, Liao Y (2020) Influence of surface roughness on contact angle hysteresis and spreading work. *Colloid Polym Sci* 298:1107–1112
- Yong M, Zhang Y, Sun S, Liu W (2019) Properties of polyvinyl chloride (PVC) ultrafiltration membrane improved by lignin: hydrophilicity and antifouling. *J Membr Sci* 575:50–59
- Zarghami S, Mohammadi T, Sadrzadeh M (2019) Preparation, characterization and fouling analysis of in-air hydrophilic/underwater oleophobic bio-inspired polydopamine coated PES membranes for oily wastewater treatment. *J Membr Sci* 582:402–413. <https://doi.org/10.1016/j.memsci.2019.04.020>
- Zhan Y et al (2021) Fabrication of durable super-hydrophilic/underwater super-oleophobic poly(arylene ether nitrile) composite membrane via biomimetic co-deposition for multi-component oily wastewater separation in harsh environments. *Colloids Surf A Physicochem Eng Aspects* 624:126754. <https://doi.org/10.1016/j.colsurfa.2021.126754>
- Zhang N et al (2022) A review on oil/water emulsion separation membrane material. *J Environ Chem Eng* 10:107257. <https://doi.org/10.1016/j.jece.2022.107257>
- Zhou L et al (2019) One-pot route to synthesize HNTs@ PVDF membrane for rapid and effective separation of emulsion-oil and dyes from waste water. *J Hazard Mater* 380:120865
- Zhu Q, Li Z (2015) Hydrogel-supported nanosized hydrous manganese dioxide: synthesis, characterization, and adsorption behavior study for Pb<sup>2+</sup>, Cu<sup>2+</sup>, Cd<sup>2+</sup> and Ni<sup>2+</sup> removal from water. *Chem Eng J* 281:69–80

**Publisher's Note** Springer Nature remains neutral with regard to jurisdictional claims in published maps and institutional affiliations.

Springer Nature or its licensor (e.g. a society or other partner) holds exclusive rights to this article under a publishing agreement with the author(s) or other rightsholder(s); author self-archiving of the accepted manuscript version of this article is solely governed by the terms of such publishing agreement and applicable law.